bioRxiv preprint doi: https://doi.org/10.1101/2025.04.17.649452; this version posted April 23, 2025. The copyright holder for this preprint (which was not certified by peer review) is the author/funder, who has granted bioRxiv a license to display the preprint in perpetuity. It is made available under a CC-BY-NC-ND 4.0 International license.

An animal-free bioprocess to synthesize 3D human matrix scaffolds using mesenchymal stromal cells

Shaianne N. Stein[1,2], Lorena R. Braid [1,2*]

[1]Simon Fraser University, Department of Molecular Biology and Biochemistry, Burnaby, BC, Canada

[2]Simon Fraser University, Centre for Cell Biology, Development and Disease, Burnaby, BC, Canada

*** Correspondence:**
Lorena R. Braid
lrbraid@sfu.ca

Keywords: Mesenchymal stromal cells (MSC), spheroid, decellularized matrix, extracellular matrix, collagen, basement membrane, animal component-free

Abstract

Basement membrane, the specialized extracellular matrix (ECM) that compartmentalizes endothelial and epithelial cells, is the final frontier in bioengineering. The fibrillar collagens (Col I and Col III) of the interstitial matrix are commonly used for tissue modeling, but the networking collagens that scaffold the basement membrane (human Col IV and Col VI) remain elusive. Commercial hydrogels like Matrigel that simulate basement membrane are ill-defined, dilute, variable and contain murine proteins. Here, we investigated whether human mesenchymal stromal cells (MSCs) could be used to produce 3D basement membrane scaffolds amenable to decellularization and downstream applications in bioengineering. Using a xeno-free, process, MSCs from placenta, umbilical cord, bone marrow and adipose tissues were cultivated as adherent multilayers or free-floating spheroids. Matrix assembly was assessed daily by fluorescence imaging and western blot, revealing *de novo,* systematic, matrix development. Notably, these scaffolds were rich in basement membrane-specific components Col IV and Col VI. Interestingly, we observed that MSCs produce distinct

bioRxiv preprint doi: https://doi.org/10.1101/2025.04.17.649452; this version posted April 23, 2025. The copyright holder for this preprint (which was not certified by peer review) is the author/funder, who has granted bioRxiv a license to display the preprint in perpetuity. It is made available under a CC-BY-NC-ND 4.0 International license.

25 combinations of Col IV alpha chains and other matrix components depending on their tissue of
26 origin. Ongoing work aims to combine this intrinsic Col IV patterning with other strategic process
27 parameters to refine basement membrane composition to resemble target tissues, and to develop
28 assays for processes like angiogenesis that incorporate relevant matrix biology as a variable and
29 readout.
30

bioRxiv preprint doi: https://doi.org/10.1101/2025.04.17.649452; this version posted April 23, 2025. The copyright holder for this preprint (which was not certified by peer review) is the author/funder, who has granted bioRxiv a license to display the preprint in perpetuity. It is made available under a CC-BY-NC-ND 4.0 International license.

Introduction

Bioengineering is a field of exponential biological innovation that is revolutionizing research and applied medicine. However, advancement of animal-free and human biomimetic biomaterials has been limited by the lack of raw materials to simulate the range of extracellular matrix (ECM) scaffolds that underlie human tissues. (Aisenbrey & Murphy, 2020; Perugini & Santin, 2021) In recent years, the critical role of ECM in fabricating high fidelity human organoids and tissues has become appreciated. (Jain et al., 2022; Kozlowski et al., 2021; Motta et al., 2023) The ECM not only serves as a scaffold that maintains the three-dimensional architecture of tissues but also influences cellular functions such as proliferation, differentiation, and migration through its biochemical composition and physical characteristics.(Olesen et al., 2021) Moreover, the mechanical properties of the ECM, such as stiffness and elasticity, significantly impact cellular behavior. (Black et al., 2008; Gonzalez-Fernandez et al., 2022; Saraswathibhatla et al., 2023; Thai et al., 2024)

Mammalian tissues and organs are scaffolded by two classes of ECM: (1) interstitial matrix and (2) basement membrane. (Pompili et al., 2021) Interstitial matrix is comprised mainly of the fibrillar collagens (I and III) and scaffolds the lamina propria, submucosa, muscular and serosa layers. (Pompili et al., 2021) The basement membrane is a specialized form of ECM located beneath the epithelial and endothelial cells that is scaffolded predominantly by the network forming collagen (Col), Col IV. (Khalilgharibi & Mao, 2021; Pompili et al., 2021) Basement membrane surrogates like Matrigel® and Cultrex™ are widely used in 3D culture. (Aisenbrey & Murphy, 2020; Kane et al., 2018) However, the biophysical, biochemical and functional properties of these matrix surrogates only distantly resemble human ECM. (Huang et al., 2021; Hughes et al., 2010; Kleinman & Martin, 2005; Kozlowski et al., 2021) These hydrogels are derived from murine Engelbreth-Holm-Swarm sarcoma (Jain et al., 2022; Kozlowski et al., 2021; Motta et al., 2023) and can contain up to 1800

bioRxiv preprint doi: https://doi.org/10.1101/2025.04.17.649452; this version posted April 23, 2025. The copyright holder for this preprint (which was not certified by peer review) is the author/funder, who has granted bioRxiv a license to display the preprint in perpetuity. It is made available under a CC-BY-NC-ND 4.0 International license.

different mouse proteins (Hughes et al., 2010) which introduce xenogeneic contaminants that that interfere with experimental veracity and that are incompatible with transplant into humans. (Aisenbrey & Murphy, 2020; de la Vega et al., 2019) While these and other biomaterials like bioinks contain soluble matrix components, they lack the structural organization that provides essential cues for tissue development and organization. (Tuftee et al., 2024) Thus, there is a critical need for animal-component free matrix scaffolds that recapitulate the architecture of native tissues.

Several approaches have been explored to address this limitation. Tissues and organs from animals and from human cadavers can be decellularized to yield intact matrix scaffolds for selective reseeding to create tissue models for experimentation (Duisit et al., 2018; Jin et al., 2022; Johnson et al., 2016) and transplant. (Griffith et al., 2022; Shaheen et al., 2020) Similarly, homogeneous and multicellular spheroids (microtissues) can be cultivated to facilitate 3D ECM synthesis followed by decellularization for downstream applications. (Chen et al., 2025; Chiang et al., 2021; Fonseca et al., 2023; Malakpour-Permlid et al., 2021; Y. Zhang et al., 2023) A recent study showed that human lung and cardiac fibroblasts from healthy and diseased donors could be used to synthesize matrix scaffolds that recapitulate the architectural features of normal and diseased lungs and hearts, respectively. (Fonseca et al., 2023; Franco-Barraza et al., 2016) Other matrix-producing cell types, including mesenchymal stromal cells (MSCs), epithelial, hepatocytes and endothelial cells have also proven useful for producing 3D matrix scaffolds with various compositions and architecture. (Fonseca et al., 2023; Pompili et al., 2021; Smith et al., 2020; Tao et al., 2020) Together, these data suggest that the range of tissue-specific matrices found throughout the human body could potentially be synthesized *in vitro* by strategic selection of cell type for 3D culture. Further refinement may also be achieved by tuning environmental conditions by addition of small molecules (Tong et al., 2018), growth factors (Gonzalez-Fernandez et al., 2016; Malakpour-Permlid et al., 2021; Seif-Naraghi et al., 2012) and

bioRxiv preprint doi: https://doi.org/10.1101/2025.04.17.649452; this version posted April 23, 2025. The copyright holder for this preprint (which was not certified by peer review) is the author/funder, who has granted bioRxiv a license to display the preprint in perpetuity. It is made available under a CC-BY-NC-ND 4.0 International license.

macromolecular crowding, for example. (Assunção et al., 2020; Chiang et al., 2021; Tao et al., 2020) Several groups have characterized how different decellularization techniques affect matrix structure and function, enabling researchers to select detergents that allow them to preserve the relevant matrix attributes necessary for their applications. (Kim et al., 2022; Crapo et al., 2011; Fonseca et al., 2023; Gilpin & Yang, 2017; Marinkovic et al., 2016, 2020; Park et al., 2018; Prewitz et al., 2013; Rakian et al., 2015).

Despite the rich potential to exploit human cells to synthesize ECM *in vitro*, most studies to date include xenogeneic components like fetal bovine serum (FBS) for cell culture. FBS remains the most widely used cell culture supplement due to its low cost and rich source of nutrients, growth factors and hormones to support mammalian cell growth and proliferation. (M. Baker, 2016b; Hemeda et al., 2014; Jung et al., 2010; Liu et al., 2023) However, many growth factors are sequestered in the matrix for on-demand release by proteases during tissue remodeling, injury and inflammation. (Keppie et al., 2021; Zhang et al., 2017) Thus, ECM cultivated in the presence of FBS contains embedded proteins of bovine origin, a concern exacerbated by the reported batch-to-batch variability of FBS. (M. Baker, 2016b, 2016a; Hemeda et al., 2014; Jung et al., 2010; Liu et al., 2023) Human platelet lysate (hPL) is a non-xenogeneic alternative to FBS for human cell culture but is also plagued by donor variability (Hemeda et al., 2014; Jung et al., 2010; Becherucci et al., 2018; Palombella et al., 2022) and is therefore not ideal for experiments and processes that require stringent reproducibility. Chemically defined culture media are emerging as an important alternative to ensure reproducible bioprocess conditions. However, these formulations are not as nutrient-rich as FBS or hPL-containing products, resulting in overall blunted cell performance. (Hemeda et al., 2014; Jung et al., 2010; Xu et al., 2020; Spoerer et al., 2025).

bioRxiv preprint doi: https://doi.org/10.1101/2025.04.17.649452; this version posted April 23, 2025. The copyright holder for this preprint (which was not certified by peer review) is the author/funder, who has granted bioRxiv a license to display the preprint in perpetuity. It is made available under a CC-BY-NC-ND 4.0 International license.

Here we tested whether human MSCs could synthesize *de novo* 3D ECM scaffolds in an animal component-free workflow. We adopted a quality-by-design approach to select only defined and qualified reagents, including MSCs, that are available in GMP-compliant formulations for further manufacturing. Several studies have already shown that MSCs synthesize a wide array of ECM constituents (Chen et al., 2025; Maia et al., 2014; Novoseletskaya et al., 2020; Sagaradze et al., 2020; Yin et al., 2024), and we previously reported that many of the potential biomarkers that distinguish MSCs from fibroblasts are linked to the matrisome. (Wiese & Braid, 2020) Fibroblasts are components of interstitial tissue and are programmed to synthesize interstitial matrix containing the fibrillar collagens 1 and 3 amongst others. (Kumada & Zhang, 2010; Wilks et al., 2018) Here we show that perinatal (umbilical cord (UC) and placental (PL)) and adult (adipose (AD) and bone marrow (BM)) derived MSCs synthesize 3D ECM in suspended and adherent chemically-defined cultures. The composition of the matrices varies by MSC tissue of origin and can include basement membrane-like scaffolds enriched for the networking collagen Col IV.

Materials and Methods

2.1 Cell source

High quality human MSCs were obtained from commercial sources. UC were provided by Tissue Regeneration Therapeutics (TRT), Inc. (Toronto, Canada). UC MSCs were isolated from the perivascular Wharton's jelly of healthy term (>37 weeks) umbilical cords from 1 male and 1 female infant delivered by C-section and cryopreserved at mean population doubling level (mPDL) 4.87. AD and BM MSCs from female donors were obtained from RoosterBio Inc. (Frederick, MD) at 8.9 and 8.8 mPDL respectively. PL MSCs from a female donor was obtained from OrganaBio (Miami, FL) at PDL 8.39. Experiments were performed using one donor population per tissue of origin.

bioRxiv preprint doi: https://doi.org/10.1101/2025.04.17.649452; this version posted April 23, 2025. The copyright holder for this preprint (which was not certified by peer review) is the author/funder, who has granted bioRxiv a license to display the preprint in perpetuity. It is made available under a CC-BY-NC-ND 4.0 International license.

126

127 2.2 Cell culture and maintenance

128 For cell expansion, MSCs were seeded at a density of 1,333 cells (UC MSCs) and 3,000 cells (AD,
129 BM, PL MSCs)/cm^2 in chemically defined phenol red-free MSC NutriStem XF® complete growth
130 media (Sartorius AG, USA). Culture-ware was pretreated with 2.67µg/cm^2 Col IV from human
131 placenta (MilliporeSigma) to facilitate adherence. Cells were maintained in physioxia at 37°C, 5%
132 CO_2, 5% O_2 and 80% relative humidity. At 70-80% confluence, MSCs were washed briefly with
133 Dulbecco's phosphate buffered saline (DPBS; MilliporeSigma) and enzymatically detached by brief
134 incubation with TrypLE Select (ThermoFisher Scientific, Waltham, MA). Upon complete
135 dissociation, an equal volume of media was added to the cell suspension and cells enumerated using
136 the CellDrop Fluorescent Cell Counter (DeNovix Inc., USA). Cells were pelleted by centrifugation at
137 150 x *g* for 5 minutes and the cell pellet resuspended in fresh chemically defined media before re-
138 seeding. All experiments were performed using MSCs between PDLs 16-24.

139 2.3 Generation of 3D MSC adherent multilayers

140 MSCs were expanded and maintained to harvest an appropriate number of cells for experiments.
141 High-density MSCs (7,813 cells/cm^2) were seeded into 24 well plates in chemically defined media
142 with media changes every 2-3 days and maintained at 37°C, 5% CO_2, 5% O_2 and 80% relative
143 humidity. At specified timepoints (days 1, 2, 4 or 7 after seeding), MSCs were washed with DPBS
144 and then decellularized (see section 2.5) for subsequent immunostaining.

145

146

147

bioRxiv preprint doi: https://doi.org/10.1101/2025.04.17.649452; this version posted April 23, 2025. The copyright holder for this preprint (which was not certified by peer review) is the author/funder, who has granted bioRxiv a license to display the preprint in perpetuity. It is made available under a CC-BY-NC-ND 4.0 International license.

2.4 Self-assembled spheroids

Spheroids were generated using a protocol adapted from Li et al (Li et al., 2021): 96-well plates were coated with 75µl of sterile 1% agarose (w/v) and allowed to solidify at room temperature. Coated plates were used immediately or stored up to 1 week in 80µl DPBS per well. DPBS was aspirated prior to seeding. MSCs were suspended in culture media at a concentration of 437,500 cells/ml (35,000 cells/well). 80µl of cell suspension was added to the coated wells and spheroids were allowed to spontaneously aggregate over 4 days. To generate spheroids of different sizes, UC MSCs were cultivated using initial cell counts of 7,000, 15,000, 35,000 or 75,000 MSCs per well.

To quantify differences in spheroid morphology across MSC tissue sources, AD, BM, PL and UC MSCs spheroids were nucleated using 35,000 cells/well. Phase contrast images were captured on days 1, 2 and 4 using an Echo Revolve inverted microscope (ECHO Inc., USA) with 10X objective for morphometric analysis.

2.5 Decellularization

Adherent multilayered MSCs were decellularized on days 1, 2, 4 and 7 after seeding. Briefly, 24 well plates were rinsed twice in DPBS, then incubated in decellularization solution (20mM NH_4OH + 0.5% Triton-X100 plus 1X cOmplete^{TM} EDTA-free protease inhibitor cocktail (Roche) for 5 minutes at 37°C, 5% CO_2, 5% O_2 and 80% relative humidity.

Spheroids were washed twice in DPBS for 5 minutes each then incubated in decellularization solution for 30 minutes at 37°C, 5% CO_2, 5% O_2 and 80% relative humidity. To remove residual DNA, the decellularized spheroids were washed twice more in DPBS, then treated with 50kU of

bioRxiv preprint doi: https://doi.org/10.1101/2025.04.17.649452; this version posted April 23, 2025. The copyright holder for this preprint (which was not certified by peer review) is the author/funder, who has granted bioRxiv a license to display the preprint in perpetuity. It is made available under a CC-BY-NC-ND 4.0 International license.

DNAseI plus EDTA-free protease inhibitor diluted in water for 30 minutes at 37°C, 5% CO_2, 5% O_2 and 80% relative humidity.

2.6 Immunofluorescence

Immunofluorescence imaging of adherent multilayer scaffolds was performed on cellularized and decellularized samples. Wells were rinsed, fixed with 10% neutral buffered formalin for 10 minutes and then permeabilized with PBT (1X DPBS + 0.1% Triton-X100) for 10 minutes followed by two phosphate buffered saline (PBS) rinses. Wells were then blocked with 10% normal donkey serum (MilliporeSigma) diluted in PBST (PBS + 0.1% Tween-20) for 30 minutes. Primary antibodies against human collagen-IV (Col IV, 1:200, NovusBio NB120-6586), laminin (LM, 1:200, NovusBio NB300-144,), fibronectin (FN, 1:200, NovusBio AF1918), and collagen-VI alpha 1 (Col VI, 1:200, NovusBio NB120-6588) were diluted in antibody dilution buffer (PBS + 0.1% Triton-X100 with 1% bovine serum albumin (BSA)) (MilliporeSigma) and incubated with the sample overnight at 4°C. Cells were washed 3 times for 5 minutes each with PBS at room temperature, then incubated for 1 hour at room temperature with secondary antibodies (donkey anti-Rabbit IgG (H+L) conjugated to AlexaFluor™ 647 (Invitrogen A32795) or donkey anti-Sheep IgG conjugated to AlexaFluor™ 594 (Invitrogen A110106)) diluted 1:1000 in antibody dilution buffer. Cells were rinsed twice with PBS and then stained with 4',6-diamidino-2-phenylindole (DAPI, 1:4000, MilliporeSigma) for 2 minutes at room temperature before washing 3 times for 5 minutes each in PBS.

Images were captured using a Nikon ECLIPSE Ti2-E inverted microscope with the 20X objective lens with 32X averaging on NIS Elements software (Nikon Instruments, Inc., USA). Images were edited using FIJI (v1.54k; (Schindelin et al., 2012)). Wells corresponding to days 1 and 2 were edited to remove background and visualize weak signal. Raw images were imported into FIJI as 16-bit,

bioRxiv preprint doi: https://doi.org/10.1101/2025.04.17.649452; this version posted April 23, 2025. The copyright holder for this preprint (which was not certified by peer review) is the author/funder, who has granted bioRxiv a license to display the preprint in perpetuity. It is made available under a CC-BY-NC-ND 4.0 International license.

greyscale images and the brightness and contrast of each image optimized: FN minimum and maximum levels were set to 185 and 400, respectively; Col IV minimum and maximum levels were set to 170 and 600, respectively; Col VI minimum and maximum levels were set to 120 and 275, respectively; LM minimum and maximum levels were set to 115 and 540, respectively. Images taken on days 4 and 7 were comparably adjusted to maintain consistency between timepoints. FN minimum and maximum levels were set to 160 and 250, respectively; Col IV minimum and maximum levels were set to 145 and 275, respectively; Col VI minimum and maximum levels were set to 125 and 200, respectively; LM minimum and maximum levels were set to 115 and 190, respectively. Z-stacked images were taken using a Nikon A1R Laser Scanning Confocal microscope equipped with a Plan Fluor 40X Oil DIC H N2 lens with cellularized UC MSCs after 7 days in culture.

Decellularization efficiency was measured using FIJI. DAPI 16-bit images were imported and threshold with black background was set for the cellularized (913-65535) and decellularized (1600 or 2724- 65535) respectively. A gaussian blur with sigma factor 2 was applied with auto thresholding set to “default dark”. The images were masked based on the thresholding values, and the “analyze particles” tool was used to obtain nuclei count. Intact nuclei were counted from at least 10 fields of view per each of 3 decellularized wells and per 1 cellularized well in each experiment. Decellularization efficiency was calculated as the percent of nuclei in decellularized wells compared to cellularized wells.

2.7 Morphometric analysis

Images were acquired on days 1, 2 and 4 as described in section 2.4 and processed using Adobe Photoshop 2023 (24.0.1, Adobe, USA). Spheroids were selected using Object Selection. In cases

bioRxiv preprint doi: https://doi.org/10.1101/2025.04.17.649452; this version posted April 23, 2025. The copyright holder for this preprint (which was not certified by peer review) is the author/funder, who has granted bioRxiv a license to display the preprint in perpetuity. It is made available under a CC-BY-NC-ND 4.0 International license.

where the background was too high for auto-selection, the Magnetic Lasso tool was used to manually trace the spheroid perimeter. The background replaced with grey as a separate layer on Photoshop to restrict calculations of each spheroid. For the initial spheroid seeding density experiments, the Ruler tool was used to measure spheroid diameter after 4 days in culture. Next, the Measure tool was used to automatically quantify spheroid area, perimeter and circularity. At least 19 spheroids per biological replicate, per tissue source were quantified.

2.8 Western blot

Total protein was collected from at least 15 pooled, decellularized and DNAseI-treated spheroids per tissue source and replicate. Decellularized spheroids were washed twice with DPBS then submerged in 75µl radioimmunoprecipitation assay (RIPA) buffer and immediately flash frozen in liquid nitrogen and stored at -80°C until use. 3D matrices were solubilized by 3 rounds of sonication at 10% amplitude for 30 seconds (1 second on, 1 off). Protein concentration was determined using Bicinchoninic acid assay (BCA; MilliporeSigma). Samples were diluted and prepared in 6X Laemmli buffer to load 3ug of total protein in 10µl per lane then boiled at 95°C before loading on an 8% gel. Proteins were subjected to electrophoresis for 1.5 hours at 140V. Size fractionated proteins were transferred to a nitrocellulose membrane overnight at 4°C. The membrane was incubated with primary antibody solution (rabbit anti-human col IV (1:1000, NovusBio, NB120-6586), rabbit anti-laminin (1:1000, NovusBio, NB300-144), rabbit anti-col VI alpha 1 (1:2000, NovusBio NB120-6588), rabbit anti Col I (1:500, Abcam ab34710), sheep anti-fibronectin (1:3000, NovusBio AF1918) or rabbit anti-elastin (1:3000, Invitrogen PA5-99418) overnight at 4°C. Membranes were then washed twice in 1X TBST for 10 minutes each, followed by blocking for 10 minutes each in 5% skim milk, and 5% BSA for elastin. Secondary antibodies (goat anti-rabbit IgG, H+L chain specific peroxidase conjugate (1:3000, Millipore Sigma 401393), rabbit anti-sheep IgG (H+L) secondary

bioRxiv preprint doi: https://doi.org/10.1101/2025.04.17.649452; this version posted April 23, 2025. The copyright holder for this preprint (which was not certified by peer review) is the author/funder, who has granted bioRxiv a license to display the preprint in perpetuity. It is made available under a CC-BY-NC-ND 4.0 International license.

antibody (1:4000,Invitrogen 61-8620) or AMDEX™ goat anti- rabbit horseradish peroxidase conjugate (1:3000, Cytiva RPN4301) were diluted in blocking solution and added to the membrane for 1 hour at room temperature. Membranes were washed four times in 1X TBS + 0.1% Triton-X100 (TBST) and visualized using UltraScence Pico Ultra Western Substrate (FroggaBio). Western blots were imaged using an Amersham™ AI600 Imager (GE HealthCare Technologies, USA).

2.9 Statistical analyses

Statistical analysis was carried out using Prism 10.3.1 (GraphPad Software, LLC). Significant differences were calculated using student's t-test (decellularization efficiency), 2-way analysis of variance (spheroid morphometrics) and Kruskal-Wallis test (spheroid initial seeding density). Error bars represent standard deviation (SD) ± of the calculated means. ns = non-significant $P>0.05$, * $P \leq 0.05$, ** $P \leq 0.01$, *** $P \leq 0.001$ and **** $P \leq 0.0001$. All experiments were performed 3 independent times.

Results

Multilayered UC MSCs produce 3D matrices in chemically defined media

We first asked whether our previously documented expression of matrisome genes by UC MSCs (Wiese & Braid, 2020) correlated with protein synthesis and could result in *de novo* production of matrices containing the basement membrane collagen Col IV in chemically defined conditions. UC MSCs were cultured in adherent multilayers followed by decellularization to assess ECM biogenesis. Ammonium hydroxide decellularization cleared 95.3% of nuclei, proving highly effective (Fig.S1). We then analyzed the deposition of select adhesive (fibronectin, laminin) and structural (Col IV) matrix

bioRxiv preprint doi: https://doi.org/10.1101/2025.04.17.649452; this version posted April 23, 2025. The copyright holder for this preprint (which was not certified by peer review) is the author/funder, who has granted bioRxiv a license to display the preprint in perpetuity. It is made available under a CC-BY-NC-ND 4.0 International license.

proteins over time by immunofluorescence. In the multilayer scaffolds, fibronectin was the most prevalent matrix component at Day 1 and increased in abundance and architectural complexity through day 7 (Fig. 1A, B). Laminin and Col IV were not detectable until Day 2, after which both proteins accumulate in networked structures through day 7 (Fig. 1A, B). Z-stacked cross-section views of day 7 cellularized cultures (Fig. 1C) reveal a matrix depth of approximately 8µm, with fibronectin interspersed throughout the scaffold (Fig. 1D). Lysl oxidase-like 2 (LOXL2), an ECM crosslinking enzyme and important for Col IV stabilization was used as a cytoplasmic marker to delineate MSCs (white) depicting them directly interacting with the fibronectin matrix (Fig. 1C, D).

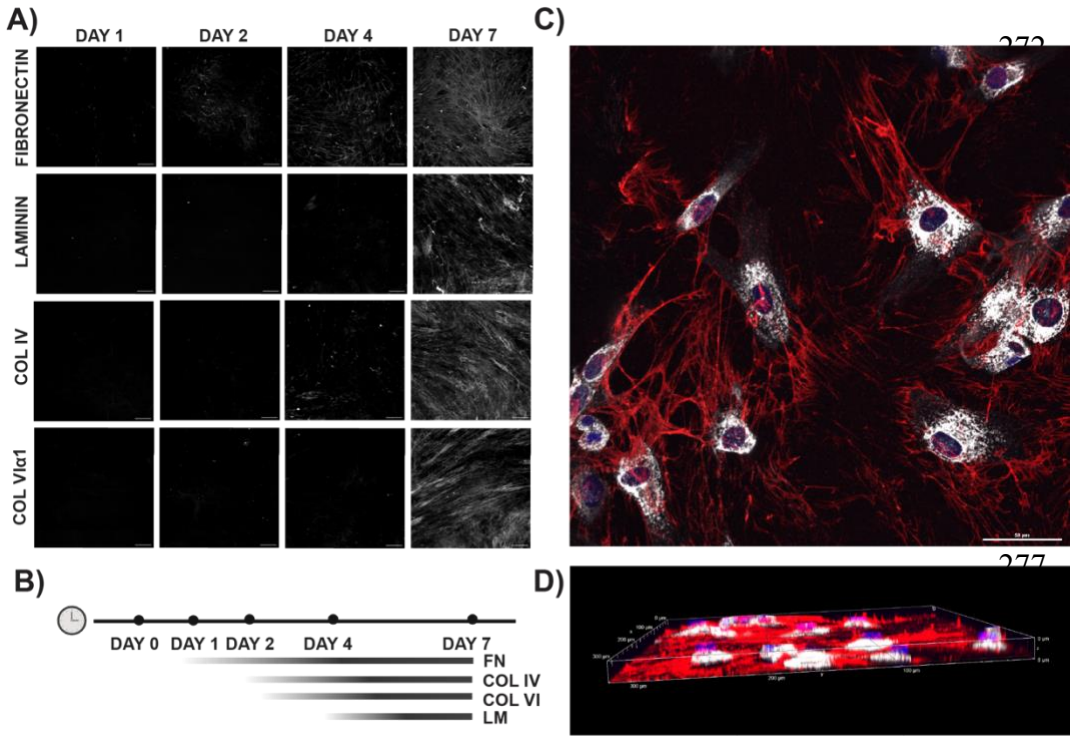


Figure 1: High-density UC MSC cultures construct 3D matrices. (A) Fibronectin is first detected by immunogenic staining 2 days after seeding, followed by Col IV on Day 4. Laminin and Col VI are not readily detected until Day 7, when all 4 analytes are visible components of an organized matrix structure. Scale bar = 100µm (B) Schematic summarizing the temporal synthesis of ECM components depicted in (A). (C) Z-stacked maximum intensity projection of cellularized adherent

bioRxiv preprint doi: https://doi.org/10.1101/2025.04.17.649452; this version posted April 23, 2025. The copyright holder for this preprint (which was not certified by peer review) is the author/funder, who has granted bioRxiv a license to display the preprint in perpetuity. It is made available under a CC-BY-NC-ND 4.0 International license.

multilayers reveal networks of fibronectin (red) networks intercalating between MSCs (white). (D) 3D adherent multilayer displayed in maximum intensity projection cross-section (volume) view shows 8 µm matrix thickness in the Z-plane. Red: fibronectin, white: LOXL2 (cytoplasmic marker), blue: DAPI (nuclear marker). Data shown is representative from a dataset of n=3 independent experiments with 5-6 fields of view per experiment.

MSCs from different human tissues self-assemble into 3D spheroids in chemically defined media

Having confirmed that UC MSCs can produce Col IV-positive matrix with scaffolded architecture, we next examined whether MSCs from adult (AD, BM) and perinatal (PL, UC) tissues could construct *de novo* 3D matrix as spheroids when cultured in chemically defined media. Within four days of high-density seeding on agarose-coated 96-well plates, MSCs from both adult and perinatal tissues formed a single free-floating spheroid in each well (Fig. 2A). A small number of unincorporated cells remained in solution and formed micro-aggregates or attached to the wall of the well, particularly in AD MSC cultures (not shown).

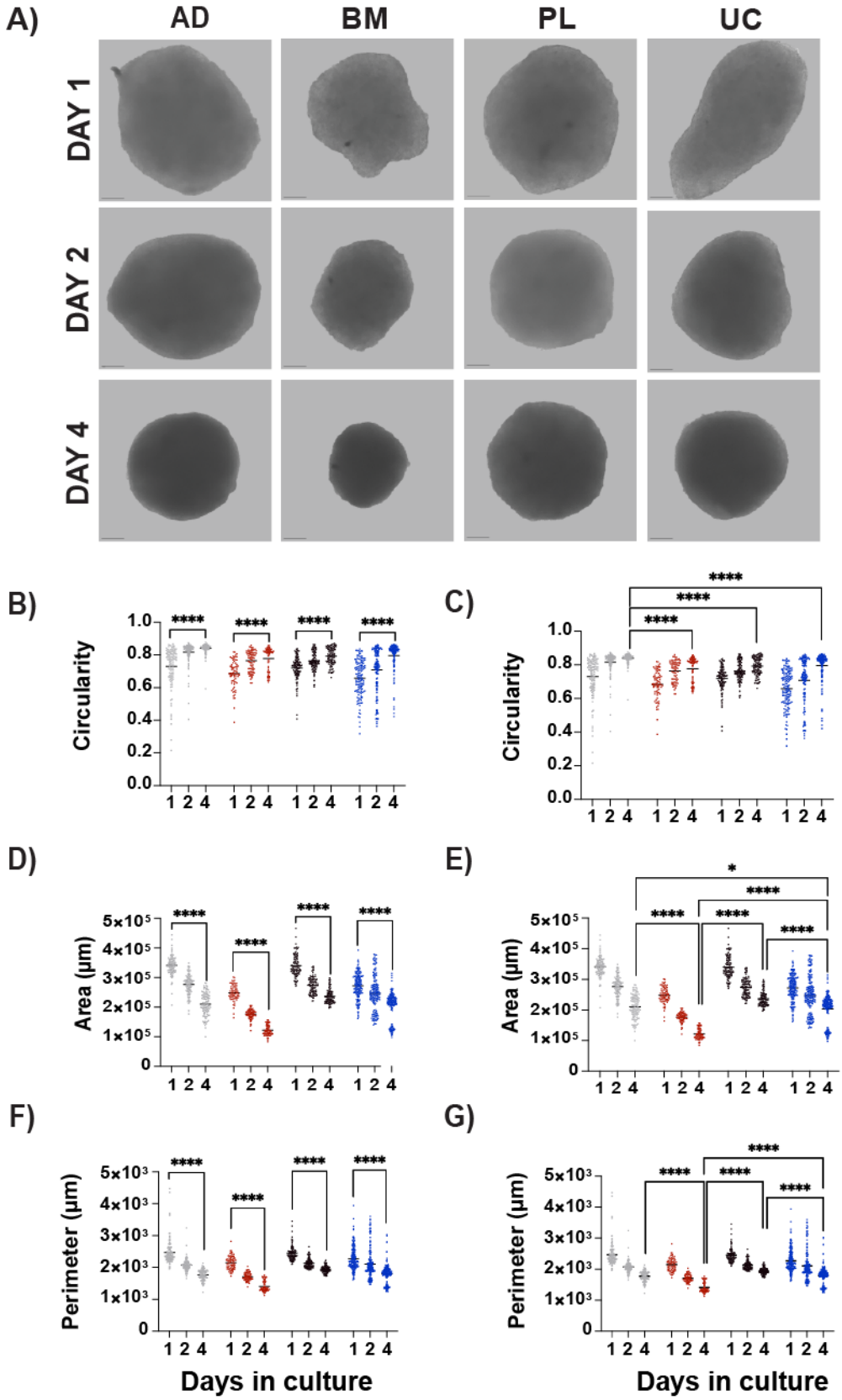
The morphometric uniformity and reproducibility of the resulting spheroids were assessed within tissue each source and between tissue sources. The spheroids become more uniform over time. Circularity (where 1.0 is a perfect circle) increases from day 1 to day 4 by 11-15% for each MSC type, resulting in average circularities of 0.84, 0.78, 0.80 and 0.80 by day 4 for AD, BM, PL and UC MSCs, respectively (Fig. 2B, C). Circularity was accompanied by compaction, as the spheroids significantly decreased in area (Fig. 2D, E) and perimeter (Fig. 2F, G). Interestingly, the rate and extent of compaction varied between MSCs from different tissues (Fig. 2C, E, G) where PL MSCs exhibited the least compaction (mean area $2.29E^5 \mu m^2$), followed by AD MSCs (mean area

bioRxiv preprint doi: https://doi.org/10.1101/2025.04.17.649452; this version posted April 23, 2025. The copyright holder for this preprint (which was not certified by peer review) is the author/funder, who has granted bioRxiv a license to display the preprint in perpetuity. It is made available under a CC-BY-NC-ND 4.0 International license.

306 2.09E^{5}µm^2). UC MSCs and BM MSCs produced the most compact spheroids with mean area
307 1.60E^{5}µm^2 and 1.20E^{5}µm^2, respectively.
308

309 We next investigated how initial cell density might influence spheroid self-assembly. Spheroids were
310 nucleated using 7,000, 15,000 35,000 and 75,000 MSCs per well. (Fig. 3A) Irrespective of seeding
311 density, all spheroids successfully self-aggregated. Spheroid size increased relative to seeding
312 density, but not linearly (Fig. 3B). All spheroids were visible by eye with diameters ranging from
313 326 to 707µm (Fig. 3A). With the exception of the largest aggregates nucleated with 75,000 cells,
314 spheroids could be aspirated using a P1000 pipette without shearing. On the other hand, the smallest
315 spheroids were challenging to visualize and manipulate. Considering these practical limitations, as
316 well as reported oxygen diffusion limits (Murphy et al., 2017), we selected spheroids nucleated using
317 35,000 MSCs and cultured to day 4 for the remainder of the study.
318

bioRxiv preprint doi: https://doi.org/10.1101/2025.04.17.649452; this version posted April 23, 2025. The copyright holder for this preprint (which was not certified by peer review) is the author/funder, who has granted bioRxiv a license to display the preprint in perpetuity. It is made available under a CC-BY-NC-ND 4.0 International license.



bioRxiv preprint doi: https://doi.org/10.1101/2025.04.17.649452; this version posted April 23, 2025. The copyright holder for this preprint (which was not certified by peer review) is the author/funder, who has granted bioRxiv a license to display the preprint in perpetuity. It is made available under a CC-BY-NC-ND 4.0 International license.

Figure 2: MSC tissue source influences spheroid morphology. A) Spheroids from AD, BM, PL and UC MSCs display variable morphology after 4 days in culture. MSC spheroids became more uniform over time as shown by changes in circularity where 1.0 is a perfect circle (B) within tissue sources and (C) across tissue sources. The increase in circularity is accompanied by an increase in compaction and a significant decrease in area (D) within tissue sources and (E) across tissue sources along with a significant decrease in perimeter (F) within tissue sources and (G) across tissue sources. At least 19 spheroids per tissue source were analyzed per experiment. Each datapoint corresponds to one spheroid from n=3 independent experiments. Scale bar = 100µm.

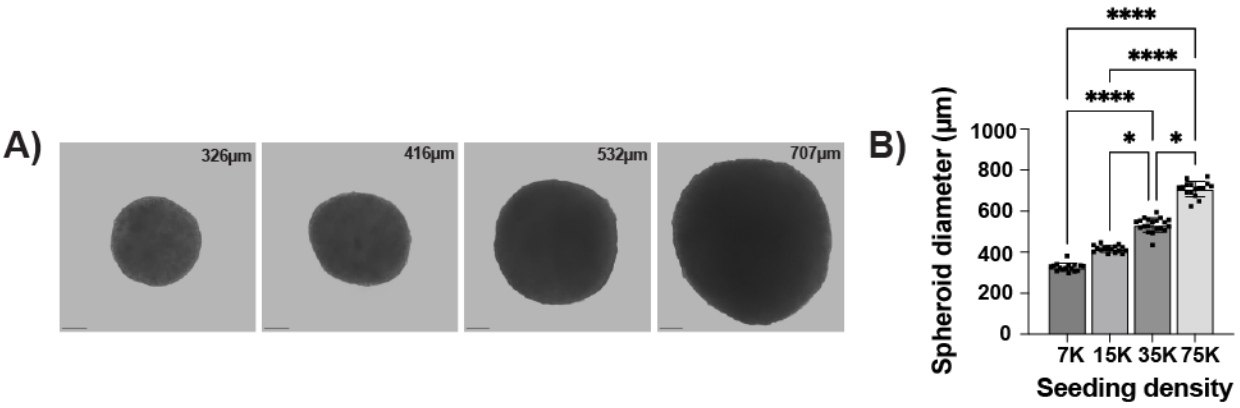


Figure 3: Spheroid diameter increases with initial seeding density. Spheroids were seeded using 7,000, 15,000, 35,000 or 75,000 US MSCs and cultivated for 4 days. (A) Diameter (upper right corner) is the average measurement for each group. (A, B) Spheroid diameter (µm) increased with seeding density.

Representative images are from n=3 independent experiments. Scale bar = 100µm.

MSCs from different tissue sources produce different levels of matrix components

We then examined how tissue of origin might influence the ability of MSCs to produce basement membrane-like ECM. Decellularized 3D spheroids were solubilized, normalized to total protein and

bioRxiv preprint doi: https://doi.org/10.1101/2025.04.17.649452; this version posted April 23, 2025. The copyright holder for this preprint (which was not certified by peer review) is the author/funder, who has granted bioRxiv a license to display the preprint in perpetuity. It is made available under a CC-BY-NC-ND 4.0 International license.

analyzed by western blot. Only UC- and AD-derived matrices contained detectable levels of all the analytes, although Col IV and elastin were less represented in the AD-derived scaffolds. All the analytes except elastin were also detected in PL-derived ECM, although Col I was more prevalent than in the other matrices. The matrix produced by BM MSCs was markedly different and comprised mainly of fibronectin with little to no Col I, Col IV or elastin. Interestingly Three Col I isoforms, sized 140, 120 and 115 kDa, were produced at different levels by AD, PL and UC MSCs. While AD MSCs produced similar levels of the isoforms, PL MSCs preferentially synthesized the 120 and 115 kDa isoforms and the 115kDa isoform was the most prominent Col I isoform in UC MSC matrix.

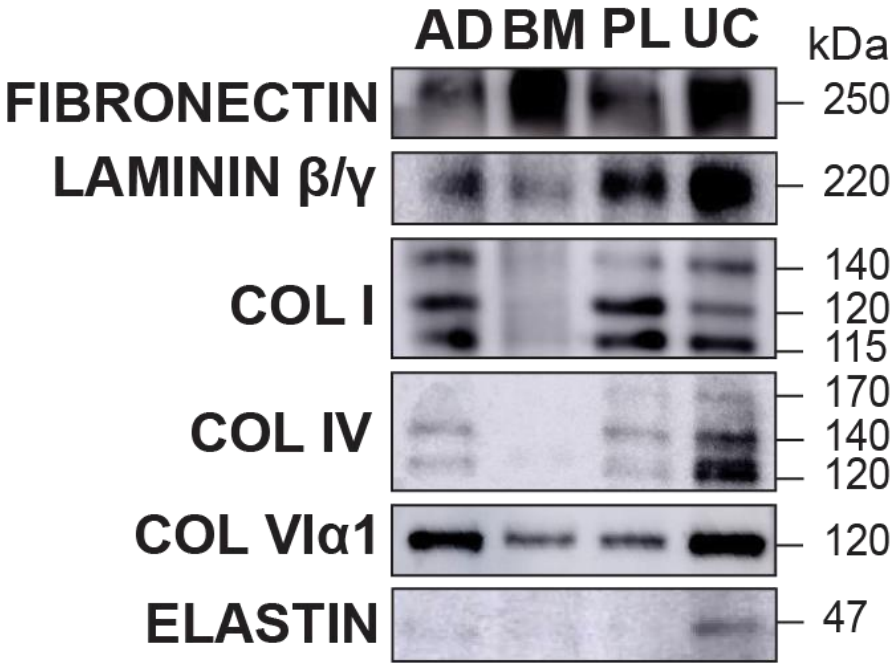


Figure 4: MSC from different tissues produce compositionally distinct matrices. Relative abundance of basement membrane proteins in decellularized AD, BM, PL or UC MSC spheroids were analyzed by western blot. Samples were normalized by total protein (3µg/lane). UC MSC matrices were enriched for all the tested basement membrane factors, although AD and PL MSCs synthesized relatively more Col I. AD and PL MSCs also produced many basement membrane factors although Col IV levels were substantially less than the other analytes. By contrast, matrix

bioRxiv preprint doi: https://doi.org/10.1101/2025.04.17.649452; this version posted April 23, 2025. The copyright holder for this preprint (which was not certified by peer review) is the author/funder, who has granted bioRxiv a license to display the preprint in perpetuity. It is made available under a CC-BY-NC-ND 4.0 International license.

357 from BM MSCs was relatively enriched for fibronectin, with negligible levels of Col I and Col IV.
358 Representative data from n=3 independent experiments.
359
360 **Discussion**
361
362 There is a critical need for functional human matrix components to support the next generation of
363 high-fidelity tissue models for experimental use and transplant. (Catarino et al., 2022; Liu et al.,
364 2023; Naderi-Meshkin et al., 2023; Schneider et al., 2023) Moreover, there is a paucity of intact and
365 functional basement membrane biomaterials to recapitulate the complexity of human tissues, and
366 more importantly, to facilitate vascularization.(Chan et al., 2016; Marrella et al., 2018; Minor &
367 Coulombe, 2020; Zhao et al., 2022) Here we report that the intrinsic architectural capacity of MSCs
368 (Kim et al., 2023; Marinkovic et al., 2020; Novoseletskaya et al., 2020; Ushakov et al., 2024; Yang et
369 al., 2024), which occupy perivascular basement membrane niches *in vivo* (Caplan, 2017; Corselli et
370 al., 2013; Kang et al., 2010) can be leveraged to synthesize basement membrane-type matrices in a
371 chemically defined bioprocess.
372
373 We performed a temporal analysis of extracellular matrix deposition and spheroid formation, studies
374 that are reportedly under-represented in the literature. (Fuentes et al., 2022) We found that MSCs
375 build 3D matrix in an organized fashion, beginning with synthesis of fibronectin. The fibronectin
376 fibers are then overlaid with laminin and Col IV, accompanied by ongoing fibronectin incorporation,
377 which recapitulates the hierarchical pattern of basement membrane synthesis *in vivo*. (Pompili et al.,
378 2021) We also documented increased spheroid organization and compaction over time, although the
379 degree of compaction was different between MSC cultures from different tissue sources. Compaction
380 is a natural developmental process that indicates organotypic self-organization. (Baker & Chen,

bioRxiv preprint doi: https://doi.org/10.1101/2025.04.17.649452; this version posted April 23, 2025. The copyright holder for this preprint (which was not certified by peer review) is the author/funder, who has granted bioRxiv a license to display the preprint in perpetuity. It is made available under a CC-BY-NC-ND 4.0 International license.

2012; Domnina et al., 2020) Spontaneous compaction, as observed here, is mainly driven by ECM structure and stiffness. (Efremov et al., 2021; Jahin et al., 2023; Kosheleva et al., 2023) we found that BM MSC-derived spheroids were significantly more compact, contained relatively more fibronectin and lacked the networking Col IV. These data suggest that BM MSC-matrices are considerably stiffer than matrices derived from UC, PL and AD MSCs, may contain high levels of other fibrillar collagens like Col III, and together are not suitable for synthesis of basement membrane-type matrices.

Indeed, we found that the synthesis and relative abundance of basement membrane components was influenced by MSC tissue of origin. Based on previous studies (Marinkovic et al., 2016, 2020; Rakian et al., 2015), including our reports that UC MSCs express significantly higher levels of the non-fibrillar basement membrane collagens (Col IV and Col VI) than fibroblasts (Wiese & Braid, 2020) and BM MSCs (Wiese et al., 2022), this outcome was anticipated. However, our results differ from some previous reports. For example, the Chen group reported that decellularized BM MSC scaffolds contained Col IV, while AD MSC scaffolds did not (Marinkovic et al., 2020), which is the inverse of our results. These disparate outcomes may be the consequence of different media formulations and FBS supplements (Bartosh et al., 2010; Cesarz & Tamama, 2016; Chen et al., 2025, 2025; Chiang et al., 2021; Fuentes et al., 2022; Lee et al., 2016; Yin et al., 2024). Only a few studies have investigated ECM synthesis in serum-free conditions (Choi et al., 2021; Rakian et al., 2015), while even fewer have used fully xeno-free processes. (Bauman et al., 2018)

Environmental conditions like oxygen tension also influence matrix synthesis. (Kumar et al., 2018; Lee et al., 2016; Satyam et al., 2016) For example, a recent study showed that human articular chondrocytes cultured at physiological oxygen tension (5% O_2) produced thicker matrices wither

bioRxiv preprint doi: https://doi.org/10.1101/2025.04.17.649452; this version posted April 23, 2025. The copyright holder for this preprint (which was not certified by peer review) is the author/funder, who has granted bioRxiv a license to display the preprint in perpetuity. It is made available under a CC-BY-NC-ND 4.0 International license.

increased deposition of glycosaminoglycans and Col II as well as increased tensile strength. (Dennis et al., 2020) MSC spheroids cultured under hypoxia (2% O_2) produced more laminin, fibronectin and Col I compared to spheroids cultured at ambient (~20%) O_2. (Shearier et al., 2016) Since MSCs were cultivated under 5% O_2 in our study, oxygen tension may be a key differential that contributes to the disparate outcomes between our data and other studies that maintain MSCs at ambient O_2 tension.

This study provides proof-of-concept that human MSCs can be leveraged to produce 3D matrices, including scaffolds enriched for basement membrane components, in an animal-component free and defined bioprocess. Subsequent work will use proteomics to comprehensively characterize the structural and signaling composition of the scaffolds. Biophysical analyses will provide further insight into how the biomechanics of these MSC-derived matrices and will inform tuning of culture conditions to more closely recapitulate *bona fide* ECM. The results herein are an in important step forward in the pursuit of high fidelity, functional tissue models for disease modeling, drug discovery and regenerative medicine.

Conflict of Interest

LRB is founder and CSO of Aurora BioSolutions Inc. SNS has no conflicts to declare. The authors declare that the research was conducted in the absence of any commercial or financial relationships that could be construed as a potential conflict of interest.

Author Contributions

SNS: Collection and/or assembly of data, data analysis and interpretation, manuscript writing, critical review of the manuscript and final approval of manuscript. LRB: Conception/design, assembly of

bioRxiv preprint doi: https://doi.org/10.1101/2025.04.17.649452; this version posted April 23, 2025. The copyright holder for this preprint (which was not certified by peer review) is the author/funder, who has granted bioRxiv a license to display the preprint in perpetuity. It is made available under a CC-BY-NC-ND 4.0 International license.

426 data, data analysis and interpretation, manuscript writing, critical review of the manuscript and final
427 approval of manuscript.

428 **Funding**

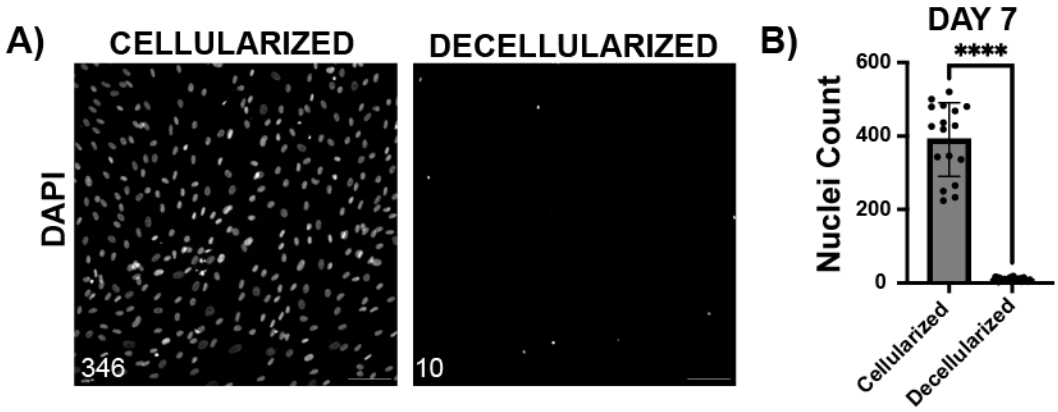
429 This project was funded by an NSERC Discovery Grant to LRB. Additional operating funds were
430 provided by a Canada Research Chair (Tier 2) in MSC Biology awarded to LRB.

431 **Acknowledgments**

432 We thank Tissue Regeneration Therapeutics Inc. (TRT), Toronto, Canada, for provision of human
433 umbilical cord perivascular cells.

434 **Supplemental Figure**

435



436
437 **Figure S1: Ammonium hydroxide decellularization efficiently clears nuclear material**.
438 Adherent 3D UC MSC cultures were decellularized using an ammonium hydroxide protocol. A)
439 Nuclei were labeled using DAPI and quantified (number in the bottom left of the image). B) The
440 number of nuclei was significantly reduced by 95.8% after decellularization.
441 Representative data from n=3 independent experiments. Scale bar = 100µm..

bioRxiv preprint doi: https://doi.org/10.1101/2025.04.17.649452; this version posted April 23, 2025. The copyright holder for this preprint (which was not certified by peer review) is the author/funder, who has granted bioRxiv a license to display the preprint in perpetuity. It is made available under a CC-BY-NC-ND 4.0 International license.

References

Aisenbrey, E. A., & Murphy, W. L. (2020). Synthetic alternatives to Matrigel. *Nature Reviews. Materials*, *5*(7), 539–551. https://doi.org/10.1038/s41578-020-0199-8

Assunção, M., Wong, C. W., Richardson, J. J., Tsang, R., Beyer, S., Raghunath, M., & Blocki, A. (2020). Macromolecular dextran sulfate facilitates extracellular matrix deposition by electrostatic interaction independent from a macromolecular crowding effect. *Materials Science & Engineering. C, Materials for Biological Applications*, *106*, 110280. https://doi.org/10.1016/j.msec.2019.110280

Baker, B. M., & Chen, C. S. (2012). Deconstructing the third dimension – how 3D culture microenvironments alter cellular cues. *Journal of Cell Science*, *125*(13), 3015–3024. https://doi.org/10.1242/jcs.079509

Baker, M. (2016a). 1,500 scientists lift the lid on reproducibility. *Nature*, *533*(7604), 452–454. https://doi.org/10.1038/533452a

Baker, M. (2016b). Reproducibility: Respect your cells! *Nature*, *537*(7620), 433–435. https://doi.org/10.1038/537433a

Bartosh, T. J., Ylöstalo, J. H., Mohammadipoor, A., Bazhanov, N., Coble, K., Claypool, K., Lee, R. H., Choi, H., & Prockop, D. J. (2010). Aggregation of human mesenchymal stromal cells (MSCs) into 3D spheroids enhances their antiinflammatory properties. *Proceedings of the National Academy of Sciences*, *107*(31), 13724–13729. https://doi.org/10.1073/pnas.1008117107

Black, L. D., Allen, P. G., Morris, S. M., Stone, P. J., & Suki, B. (2008). Mechanical and Failure Properties of Extracellular Matrix Sheets as a Function of Structural Protein Composition. *Biophysical Journal*, *94*(5), 1916–1929. https://doi.org/10.1529/biophysj.107.107144

bioRxiv preprint doi: https://doi.org/10.1101/2025.04.17.649452; this version posted April 23, 2025. The copyright holder for this preprint (which was not certified by peer review) is the author/funder, who has granted bioRxiv a license to display the preprint in perpetuity. It is made available under a CC-BY-NC-ND 4.0 International license.

Caplan, A. I. (2017). New MSC: MSCs as pericytes are Sentinels and gatekeepers. *Journal of Orthopaedic Research: Official Publication of the Orthopaedic Research Society*, *35*(6), 1151–1159. https://doi.org/10.1002/jor.23560

Catarino, C. M., Kaiser, K., Baltazar, T., Catarino, L. M., Brewer, J. R., & Karande, P. (2022). Evaluation of native and non-native biomaterials for engineering human skin tissue. *Bioengineering & Translational Medicine*, *7*(3), e10297. https://doi.org/10.1002/btm2.10297

Cesarz, Z., & Tamama, K. (2016). Spheroid Culture of Mesenchymal Stem Cells. *Stem Cells International*, *2016*, 9176357. https://doi.org/10.1155/2016/9176357

Chan, E. C., Kuo, S.-M., Kong, A. M., Morrison, W. A., Dusting, G. J., Mitchell, G. M., Lim, S. Y., & Liu, G.-S. (2016). Three Dimensional Collagen Scaffold Promotes Intrinsic Vascularisation for Tissue Engineering Applications. *PLOS ONE*, *11*(2), e0149799. https://doi.org/10.1371/journal.pone.0149799

Chen, G. H., Sia, K.-C., Liu, S.-W., Kao, Y.-C., Yang, P.-C., Ho, C.-H., Huang, S.-C., Lee, P.-Y., Liang, M.-Z., Chen, L., & Huang, C.-C. (2025). Implantation of MSC spheroid-derived 3D decellularized ECM enriched with the MSC secretome ameliorates traumatic brain injury and promotes brain repair. *Biomaterials*, *315*, 122941. https://doi.org/10.1016/j.biomaterials.2024.122941

Chiang, C.-E., Fang, Y.-Q., Ho, C.-T., Assunção, M., Lin, S.-J., Wang, Y.-C., Blocki, A., & Huang, C.-C. (2021). Bioactive Decellularized Extracellular Matrix Derived from 3D Stem Cell Spheroids under Macromolecular Crowding Serves as a Scaffold for Tissue Engineering. *Advanced Healthcare Materials*, *10*(11), e2100024. https://doi.org/10.1002/adhm.202100024

Choi, J., Choi, W., Joo, Y., Chung, H., Kim, D., Oh, S. J., & Kim, S.-H. (2021). FGF2-primed 3D spheroids producing IL-8 promote therapeutic angiogenesis in murine hindlimb ischemia. *NPJ Regenerative Medicine*, *6*, 48. https://doi.org/10.1038/s41536-021-00159-7

bioRxiv preprint doi: https://doi.org/10.1101/2025.04.17.649452; this version posted April 23, 2025. The copyright holder for this preprint (which was not certified by peer review) is the author/funder, who has granted bioRxiv a license to display the preprint in perpetuity. It is made available under a CC-BY-NC-ND 4.0 International license.

Corselli, M., Crisan, M., Murray, I. R., West, C. C., Scholes, J., Codrea, F., Khan, N., & Péault, B. (2013). Identification of perivascular mesenchymal stromal/stem cells by flow cytometry. *Cytometry. Part A: The Journal of the International Society for Analytical Cytology*, *83*(8), 714–720. https://doi.org/10.1002/cyto.a.22313

Crapo, P. M., Gilbert, T. W., & Badylak, S. F. (2011). An overview of tissue and whole organ decellularization processes. *Biomaterials*, *32*(12), 3233–3243. https://doi.org/10.1016/j.biomaterials.2011.01.057

de la Vega, L., Lee, C., Sharma, R., Amereh, M., & Willerth, S. M. (2019). 3D bioprinting models of neural tissues: The current state of the field and future directions. *Brain Research Bulletin*, *150*, 240–249. https://doi.org/10.1016/j.brainresbull.2019.06.007

Dennis, J. E., Whitney, G. A., Rai, J., Fernandes, R. J., & Kean, T. J. (2020). Physioxia Stimulates Extracellular Matrix Deposition and Increases Mechanical Properties of Human Chondrocyte-Derived Tissue-Engineered Cartilage. *Frontiers in Bioengineering and Biotechnology*, *8*. https://doi.org/10.3389/fbioe.2020.590743

Domnina, A., Ivanova, J., Alekseenko, L., Kozhukharova, I., Borodkina, A., Pugovkina, N., Smirnova, I., Lyublinskaya, O., Fridlyanskaya, I., & Nikolsky, N. (2020). Three-Dimensional Compaction Switches Stress Response Programs and Enhances Therapeutic Efficacy of Endometrial Mesenchymal Stem/Stromal Cells. *Frontiers in Cell and Developmental Biology*, *8*, 473. https://doi.org/10.3389/fcell.2020.00473

Duisit, J., Amiel, H., Wüthrich, T., Taddeo, A., Dedriche, A., Destoop, V., Pardoen, T., Bouzin, C., Joris, V., Magee, D., Vögelin, E., Harriman, D., Dessy, C., Orlando, G., Behets, C., Rieben, R., Gianello, P., & Lengelé, B. (2018). Perfusion-decellularization of human ear grafts enables ECM-based scaffolds for auricular vascularized composite tissue engineering. *Acta Biomaterialia*, *73*, 339–354. https://doi.org/10.1016/j.actbio.2018.04.009

bioRxiv preprint doi: https://doi.org/10.1101/2025.04.17.649452; this version posted April 23, 2025. The copyright holder for this preprint (which was not certified by peer review) is the author/funder, who has granted bioRxiv a license to display the preprint in perpetuity. It is made available under a CC-BY-NC-ND 4.0 International license.

513 Efremov, Y. M., Zurina, I. M., Presniakova, V. S., Kosheleva, N. V., Butnaru, D. V., Svistunov, A.
514 A., Rochev, Y. A., & Timashev, P. S. (2021). Mechanical properties of cell sheets and
515 spheroids: The link between single cells and complex tissues. *Biophysical Reviews*, *13*(4),
516 541–561. https://doi.org/10.1007/s12551-021-00821-w
517 Fonseca, V. C., Van, V., & Ip, B. C. (2023). *Primary Human Cell-Derived Extracellular Matrix from*
518 *Decellularized Fibroblast Microtissues with Tissue-Dependent Composition and*
519 *Microstructure* (p. 2023.08.15.553420). bioRxiv. https://doi.org/10.1101/2023.08.15.553420
520 Franco-Barraza, J., Beacham, D. A., Amatangelo, M. D., & Cukierman, E. (2016). Preparation of
521 Extracellular Matrices Produced by Cultured and Primary Fibroblasts. *Current Protocols in*
522 *Cell Biology*, *71*, 10.9.1-10.9.34. https://doi.org/10.1002/cpcb.2
523 Fuentes, P., Torres, M. J., Arancibia, R., Aulestia, F., Vergara, M., Carrión, F., Osses, N., &
524 Altamirano, C. (2022). Dynamic Culture of Mesenchymal Stromal/Stem Cell Spheroids and
525 Secretion of Paracrine Factors. *Frontiers in Bioengineering and Biotechnology*, *10*, 916229.
526 https://doi.org/10.3389/fbioe.2022.916229
527 Gilpin, A., & Yang, Y. (2017). Decellularization Strategies for Regenerative Medicine: From
528 Processing Techniques to Applications. *BioMed Research International*, *2017*, 9831534.
529 https://doi.org/10.1155/2017/9831534
530 Gonzalez-Fernandez, T., Tenorio, A. J., Saiz, A. M., & Leach, J. K. (2022). Engineered Cell-Secreted
531 Extracellular Matrix Modulates Cell Spheroid Mechanosensing and Amplifies Their
532 Response to Inductive Cues for the Formation of Mineralized Tissues. *Advanced Healthcare*
533 *Materials*, *11*(10), e2102337. https://doi.org/10.1002/adhm.202102337
534 Gonzalez-Fernandez, T., Tierney, E. G., Cunniffe, G. M., O'Brien, F. J., & Kelly, D. J. (2016). Gene
535 Delivery of TGF-β3 and BMP2 in an MSC-Laden Alginate Hydrogel for Articular Cartilage

bioRxiv preprint doi: https://doi.org/10.1101/2025.04.17.649452; this version posted April 23, 2025. The copyright holder for this preprint (which was not certified by peer review) is the author/funder, who has granted bioRxiv a license to display the preprint in perpetuity. It is made available under a CC-BY-NC-ND 4.0 International license.

and Endochondral Bone Tissue Engineering. *Tissue Engineering. Part A*, *22*(9–10), 776–787. https://doi.org/10.1089/ten.TEA.2015.0576

Griffith, B. P., Goerlich, C. E., Singh, A. K., Rothblatt, M., Lau, C. L., Shah, A., Lorber, M., Grazioli, A., Saharia, K. K., Hong, S. N., Joseph, S. M., Ayares, D., & Mohiuddin, M. M. (2022). Genetically Modified Porcine-to-Human Cardiac Xenotransplantation. *New England Journal of Medicine*, *387*(1), 35–44. https://doi.org/10.1056/NEJMoa2201422

Hemeda, H., Giebel, B., & Wagner, W. (2014). Evaluation of human platelet lysate versus fetal bovine serum for culture of mesenchymal stromal cells. *Cytotherapy*, *16*(2), 170–180. https://doi.org/10.1016/j.jcyt.2013.11.004

Huang, J., Zhang, L., Wan, D., Zhou, L., Zheng, S., Lin, S., & Qiao, Y. (2021). Extracellular matrix and its therapeutic potential for cancer treatment. *Signal Transduction and Targeted Therapy*, *6*, 153. https://doi.org/10.1038/s41392-021-00544-0

Hughes, C. S., Postovit, L. M., & Lajoie, G. A. (2010). Matrigel: A complex protein mixture required for optimal growth of cell culture. *Proteomics*, *10*(9), 1886–1890. https://doi.org/10.1002/pmic.200900758

Jahin, I., Phillips, T., Marcotti, S., Gorey, M.-A., Cox, S., & Parsons, M. (2023). Extracellular matrix stiffness activates mechanosensitive signals but limits breast cancer cell spheroid proliferation and invasion. *Frontiers in Cell and Developmental Biology*, *11*. https://doi.org/10.3389/fcell.2023.1292775

Jain, P., Rauer, S. B., Möller, M., & Singh, S. (2022). Mimicking the Natural Basement Membrane for Advanced Tissue Engineering. *Biomacromolecules*, *23*(8), 3081–3103. https://doi.org/10.1021/acs.biomac.2c00402

Jin, Y., Kim, H., Min, S., Choi, Y. S., Seo, S. J., Jeong, E., Kim, S. K., Lee, H.-A., Jo, S.-H., Park, J.-H., Park, B.-W., Sim, W.-S., Kim, J.-J., Ban, K., Kim, Y.-G., Park, H.-J., & Cho, S.-W.

bioRxiv preprint doi: https://doi.org/10.1101/2025.04.17.649452; this version posted April 23, 2025. The copyright holder for this preprint (which was not certified by peer review) is the author/funder, who has granted bioRxiv a license to display the preprint in perpetuity. It is made available under a CC-BY-NC-ND 4.0 International license.

(2022). Three-dimensional heart extracellular matrix enhances chemically induced direct cardiac reprogramming. *Science Advances*, *8*(50), eabn5768. https://doi.org/10.1126/sciadv.abn5768

Johnson, T. D., Hill, R. C., Dzieciatkowska, M., Nigam, V., Behfar, A., Christman, K. L., & Hansen, K. C. (2016). Quantification of Decellularized Human Myocardial Matrix: A Comparison of Six Patients. *Proteomics. Clinical Applications*, *10*(1), 75–83. https://doi.org/10.1002/prca.201500048

Jung, S., Sen, A., Rosenberg, L., & Behie, L. A. (2010). Identification of growth and attachment factors for the serum-free isolation and expansion of human mesenchymal stromal cells. *Cytotherapy*, *12*(5), 637–657. https://doi.org/10.3109/14653249.2010.495113

Kane, K. I. W., Lucumi Moreno, E., Lehr, C. M., Hachi, S., Dannert, R., Sanctuary, R., Wagner, C., Fleming, R. M. T., & Baller, J. (2018). Determination of the rheological properties of Matrigel for optimum seeding conditions in microfluidic cell cultures. *AIP Advances*, *8*(12), 125332. https://doi.org/10.1063/1.5067382

Kang, S.-G., Shinojima, N., Hossain, A., Gumin, J., Yong, R. L., Colman, H., Marini, F., Andreeff, M., & Lang, F. F. (2010). Isolation and Perivascular Localization of Mesenchymal Stem Cells From Mouse Brain. *Neurosurgery*, *67*(3), 711–720. https://doi.org/10.1227/01.NEU.0000377859.06219.78

Keppie, S. J., Mansfield, J. C., Tang, X., Philp, C. J., Graham, H. K., Önnerfjord, P., Wall, A., McLean, C., Winlove, C. P., Sherratt, M. J., Pavlovskaya, G. E., & Vincent, T. L. (2021). Matrix-Bound Growth Factors are Released upon Cartilage Compression by an Aggrecan-Dependent Sodium Flux that is Lost in Osteoarthritis. *Function*, *2*(5), zqab037. https://doi.org/10.1093/function/zqab037

bioRxiv preprint doi: https://doi.org/10.1101/2025.04.17.649452; this version posted April 23, 2025. The copyright holder for this preprint (which was not certified by peer review) is the author/funder, who has granted bioRxiv a license to display the preprint in perpetuity. It is made available under a CC-BY-NC-ND 4.0 International license.

583 Khalilgharibi, N., & Mao, Y. (2021). To form and function: On the role of basement membrane
584 mechanics in tissue development, homeostasis and disease. *Open Biology*, *11*(2), 200360.
585 https://doi.org/10.1098/rsob.200360
586 Kim, M.-H., Tan, S. Y., Yamahara, K., & Kino-oka, M. (2023). An *in vitro* culture platform to study
587 the extracellular matrix remodeling potential of human mesenchymal stem cells. *Acta*
588 *Biomaterialia*, *170*, 376–388. https://doi.org/10.1016/j.actbio.2023.08.035
589 Kleinman, H. K., & Martin, G. R. (2005). Matrigel: Basement membrane matrix with biological
590 activity. *Seminars in Cancer Biology*, *15*(5), 378–386.
591 https://doi.org/10.1016/j.semcancer.2005.05.004
592 Kosheleva, N. V., Efremov, Y. M., Koteneva, P. I., Ilina, I. V., Zurina, I. M., Bikmulina, P. Y.,
593 Shpichka, A. I., & Timashev, P. S. (2023). Building a tissue: Mesenchymal and epithelial cell
594 spheroids mechanical properties at micro- and nanoscale. *Acta Biomaterialia*, *165*, 140–152.
595 https://doi.org/10.1016/j.actbio.2022.09.051
596 Kozlowski, M. T., Crook, C. J., & Ku, H. T. (2021). Towards organoid culture without Matrigel.
597 *Communications Biology*, *4*(1), 1387. https://doi.org/10.1038/s42003-021-02910-8
598 Kumada, Y., & Zhang, S. (2010). Significant Type I and Type III Collagen Production from Human
599 Periodontal Ligament Fibroblasts in 3D Peptide Scaffolds without Extra Growth Factors.
600 *PLOS ONE*, *5*(4), e10305. https://doi.org/10.1371/journal.pone.0010305
601 Kumar, P., Satyam, A., Cigognini, D., Pandit, A., & Zeugolis, D. I. (2018). Low oxygen tension and
602 macromolecular crowding accelerate extracellular matrix deposition in human corneal
603 fibroblast culture. *Journal of Tissue Engineering and Regenerative Medicine*, *12*(1), 6–18.
604 https://doi.org/10.1002/term.2283

bioRxiv preprint doi: https://doi.org/10.1101/2025.04.17.649452; this version posted April 23, 2025. The copyright holder for this preprint (which was not certified by peer review) is the author/funder, who has granted bioRxiv a license to display the preprint in perpetuity. It is made available under a CC-BY-NC-ND 4.0 International license.

605 Lee, J. H., Han, Y.-S., & Lee, S. H. (2016). Long-Duration Three-Dimensional Spheroid Culture
606 Promotes Angiogenic Activities of Adipose-Derived Mesenchymal Stem Cells. *Biomolecules*
607 *& Therapeutics*, *24*(3), 260. https://doi.org/10.4062/biomolther.2015.146
608 Li, M., Fu, T., Yang, S., Pan, L., Tang, J., Chen, M., Liang, P., Gao, Z., & Guo, L. (2021). Agarose-
609 based spheroid culture enhanced stemness and promoted odontogenic differentiation potential
610 of human dental follicle cells in vitro. *In Vitro Cellular & Developmental Biology. Animal*,
611 *57*(6), 620–630. https://doi.org/10.1007/s11626-021-00591-5
612 Liu, S., Yang, W., Li, Y., & Sun, C. (2023). Fetal bovine serum, an important factor affecting the
613 reproducibility of cell experiments. *Scientific Reports*, *13*, 1942.
614 https://doi.org/10.1038/s41598-023-29060-7
615 Maia, F. R., Fonseca, K. B., Rodrigues, G., Granja, P. L., & Barrias, C. C. (2014). Matrix-driven
616 formation of mesenchymal stem cell–extracellular matrix microtissues on soft alginate
617 hydrogels. *Acta Biomaterialia*, *10*(7), 3197–3208.
618 https://doi.org/10.1016/j.actbio.2014.02.049
619 Malakpour-Permlid, A., Buzzi, I., Hegardt, C., Johansson, F., & Oredsson, S. (2021). Identification
620 of extracellular matrix proteins secreted by human dermal fibroblasts cultured in 3D
621 electrospun scaffolds. *Scientific Reports*, *11*(1), 6655. https://doi.org/10.1038/s41598-021-
622 85742-0
623 Marinkovic, M., Block, T. J., Rakian, R., Li, Q., Wang, E., Reilly, M. A., Dean, D. D., & Chen, X.-
624 D. (2016). One size does not fit all: Developing a cell-specific niche for in vitro study of cell
625 behavior. *Matrix Biology : Journal of the International Society for Matrix Biology*, *52–54*,
626 426–441. https://doi.org/10.1016/j.matbio.2016.01.004
627 Marinkovic, M., Tran, O. N., Block, T. J., Rakian, R., Gonzalez, A. O., Dean, D. D., Yeh, C.-K., &
628 Chen, X.-D. (2020). Native extracellular matrix, synthesized ex vivo by bone marrow or

bioRxiv preprint doi: https://doi.org/10.1101/2025.04.17.649452; this version posted April 23, 2025. The copyright holder for this preprint (which was not certified by peer review) is the author/funder, who has granted bioRxiv a license to display the preprint in perpetuity. It is made available under a CC-BY-NC-ND 4.0 International license.

adipose stromal cells, faithfully directs mesenchymal stem cell differentiation. *Matrix Biology Plus*, *8*, 100044. https://doi.org/10.1016/j.mbplus.2020.100044

Marrella, A., Lee, T. Y., Lee, D. H., Karuthedom, S., Syla, D., Chawla, A., Khademhosseini, A., & Jang, H. L. (2018). Engineering vascularized and innervated bone biomaterials for improved skeletal tissue regeneration. *Materials Today*, *21*(4), 362–376. https://doi.org/10.1016/j.mattod.2017.10.005

Minor, A. J., & Coulombe, K. L. K. (2020). Engineering a collagen matrix for cell-instructive regenerative angiogenesis. *Journal of Biomedical Materials Research Part B: Applied Biomaterials*, *108*(6), 2407–2416. https://doi.org/10.1002/jbm.b.34573

Motta, L. C. B., Pereira, V. M., Pinto, P. A. F., Mançanares, C. A. F., Pieri, N. C. G., de Olveira, V. C., Fantinato-Neto, P., & Ambrósio, C. E. (2023). 3D culture of mesenchymal stem cells from the yolk sac to generate intestinal organoid. *Theriogenology*, *209*. https://doi.org/10.1016/j.theriogenology.2023.06.003

Murphy, K. C., Hung, B. P., Browne-Bourne, S., Zhou, D., Yeung, J., Genetos, D. C., & Leach, J. K. (2017). Measurement of oxygen tension within mesenchymal stem cell spheroids. *Journal of The Royal Society Interface*, *14*(127), 20160851. https://doi.org/10.1098/rsif.2016.0851

Naderi-Meshkin, H., Cornelius, V. A., Eleftheriadou, M., Potel, K. N., Setyaningsih, W. A. W., & Margariti, A. (2023). Vascular organoids: Unveiling advantages, applications, challenges, and disease modelling strategies. *Stem Cell Research & Therapy*, *14*(1), 292. https://doi.org/10.1186/s13287-023-03521-2

Novoseletskaya, E., Grigorieva, O., Nimiritsky, P., Basalova, N., Eremichev, R., Milovskaya, I., Kulebyakin, K., Kulebyakina, M., Rodionov, S., Omelyanenko, N., & Efimenko, A. (2020). Mesenchymal Stromal Cell-Produced Components of Extracellular Matrix Potentiate

bioRxiv preprint doi: https://doi.org/10.1101/2025.04.17.649452; this version posted April 23, 2025. The copyright holder for this preprint (which was not certified by peer review) is the author/funder, who has granted bioRxiv a license to display the preprint in perpetuity. It is made available under a CC-BY-NC-ND 4.0 International license.

Multipotent Stem Cell Response to Differentiation Stimuli. *Frontiers in Cell and Developmental Biology*, *8*, 555378. https://doi.org/10.3389/fcell.2020.555378

Olesen, K., Rodin, S., Mak, W. C., Felldin, U., Österholm, C., Tilevik, A., & Grinnemo, K.-H. (2021). Spatiotemporal Extracellular Matrix Modeling for in Situ Cell Niche Studies. *Stem Cells*, *39*(12), 1751–1765. https://doi.org/10.1002/stem.3448

Park, J., Kim, J., Sullivan, K. M., Baik, S., Ko, E., Kim, M.-J., Kim, Y. J., & Kong, H. (2018). Decellularized Matrix Produced by Mesenchymal Stem Cells Modulates Growth and Metabolic Activity of Hepatic Cell Cluster. *ACS Biomaterials Science & Engineering*, *4*(2), 456–462. https://doi.org/10.1021/acsbiomaterials.7b00494

Perugini, V., & Santin, M. (2021). A Substrate-Mimicking Basement Membrane Drives the Organization of Human Mesenchymal Stromal Cells and Endothelial Cells Into Perivascular Niche-Like Structures. *Frontiers in Cell and Developmental Biology*, *9*, 701842. https://doi.org/10.3389/fcell.2021.701842

Pompili, S., Latella, G., Gaudio, E., Sferra, R., & Vetuschi, A. (2021). The Charming World of the Extracellular Matrix: A Dynamic and Protective Network of the Intestinal Wall. *Frontiers in Medicine*, *8*. https://doi.org/10.3389/fmed.2021.610189

Prewitz, M. C., Seib, F. P., von Bonin, M., Friedrichs, J., Stißel, A., Niehage, C., Müller, K., Anastassiadis, K., Waskow, C., Hoflack, B., Bornhäuser, M., & Werner, C. (2013). Tightly anchored tissue-mimetic matrices as instructive stem cell microenvironments. *Nature Methods*, *10*(8), 788–794. https://doi.org/10.1038/nmeth.2523

Rakian, R., Block, T. J., Johnson, S. M., Marinkovic, M., Wu, J., Dai, Q., Dean, D. D., & Chen, X.-D. (2015). Native extracellular matrix preserves mesenchymal stem cell “stemness” and differentiation potential under serum-free culture conditions. *Stem Cell Research & Therapy*, *6*, 235. https://doi.org/10.1186/s13287-015-0235-6

bioRxiv preprint doi: https://doi.org/10.1101/2025.04.17.649452; this version posted April 23, 2025. The copyright holder for this preprint (which was not certified by peer review) is the author/funder, who has granted bioRxiv a license to display the preprint in perpetuity. It is made available under a CC-BY-NC-ND 4.0 International license.

676 Sagaradze, G. D., Basalova, N. A., Efimenko, A. Y., & Tkachuk, V. A. (2020). Mesenchymal
677 Stromal Cells as Critical Contributors to Tissue Regeneration. *Frontiers in Cell and*
678 *Developmental Biology*, *8*. https://doi.org/10.3389/fcell.2020.576176
679 Saraswathibhatla, A., Indana, D., & Chaudhuri, O. (2023). Cell–extracellular matrix
680 mechanotransduction in 3D. *Nature Reviews. Molecular Cell Biology*, *24*(7), 495–516.
681 https://doi.org/10.1038/s41580-023-00583-1
682 Satyam, A., Kumar, P., Cigognini, D., Pandit, A., & Zeugolis, D. I. (2016). Low, but not too low,
683 oxygen tension and macromolecular crowding accelerate extracellular matrix deposition in
684 human dermal fibroblast culture. *Acta Biomaterialia*, *44*, 221–231.
685 https://doi.org/10.1016/j.actbio.2016.08.008
686 Schindelin, J., Arganda-Carreras, I., Frise, E., Kaynig, V., Longair, M., Pietzsch, T., Preibisch, S.,
687 Rueden, C., Saalfeld, S., Schmid, B., Tinevez, J.-Y., White, D. J., Hartenstein, V., Eliceiri,
688 K., Tomancak, P., & Cardona, A. (2012). Fiji: An open-source platform for biological-image
689 analysis. *Nature Methods*, *9*(7), 676–682. https://doi.org/10.1038/nmeth.2019
690 Schneider, K. H., Goldberg, B. J., Hasturk, O., Mu, X., Dötzlhofer, M., Eder, G., Theodossiou, S.,
691 Pichelkastner, L., Riess, P., Rohringer, S., Kiss, H., Teuschl-Woller, A. H., Fitzpatrick, V.,
692 Enayati, M., Podesser, B. K., Bergmeister, H., & Kaplan, D. L. (2023). Silk fibroin, gelatin,
693 and human placenta extracellular matrix-based composite hydrogels for 3D bioprinting and
694 soft tissue engineering. *Biomaterials Research*, *27*(1), 117. https://doi.org/10.1186/s40824-
695 023-00431-5
696 Seif-Naraghi, S. B., Horn, D., Schup-Magoffin, P. A., & Christman, K. L. (2012). Injectable
697 extracellular matrix derived hydrogel provides a platform for enhanced retention and delivery
698 of a heparin-binding growth factor. *Acta Biomaterialia*, *8*(10), 3695–3703.
699 https://doi.org/10.1016/j.actbio.2012.06.030

bioRxiv preprint doi: https://doi.org/10.1101/2025.04.17.649452; this version posted April 23, 2025. The copyright holder for this preprint (which was not certified by peer review) is the author/funder, who has granted bioRxiv a license to display the preprint in perpetuity. It is made available under a CC-BY-NC-ND 4.0 International license.

Shaheen, M. F., Joo, D., Ross, J. J., Anderson, B. D., Chen, H. S., Huebert, R. C., Li, Y., Amiot, B., Young, A., Zlochiver, V., Nelson, E., Mounajjed, T., Dietz, A. B., Michalak, G., Steiner, B. G., Davidow, D. S., Paradise, C. R., van Wijnen, A. J., Shah, V. H., … Nyberg, S. L. (2020). Sustained perfusion of revascularized bioengineered livers heterotopically transplanted into immunosuppressed pigs. *Nature Biomedical Engineering*, *4*(4), 437–445. https://doi.org/10.1038/s41551-019-0460-x

Shearier, E., Xing, Q., Qian, Z., & Zhao, F. (2016). Physiologically Low Oxygen Enhances Biomolecule Production and Stemness of Mesenchymal Stem Cell Spheroids. *Tissue Engineering. Part C, Methods*, *22*(4), 360. https://doi.org/10.1089/ten.tec.2015.0465

Smith, A., Huang, M., Watkins, T., Burguin, F., Baskin, J., & Garlick, J. A. (2020). De novo production of human extracellular matrix supports increased throughput and cellular complexity in 3D skin equivalent model. *Journal of Tissue Engineering and Regenerative Medicine*, *14*(8), 1019–1027. https://doi.org/10.1002/term.3071

Tao, F., Sayo, K., Sugimoto, K., Aoki, S., & Kojima, N. (2020). Development of a tunable method to generate various three-dimensional microstructures by replenishing macromolecules such as extracellular matrix components and polysaccharides. *Scientific Reports*, *10*, 6567. https://doi.org/10.1038/s41598-020-63621-4

Thai, V. L., Mierswa, S., Griffin, K. H., Boerckel, J. D., & Leach, J. K. (2024). Mechanoregulation of MSC spheroid immunomodulation. *APL Bioengineering*, *8*(1), 016116. https://doi.org/10.1063/5.0184431

Tong, Z., Martyn, K., Yang, A., Yin, X., Mead, B. E., Joshi, N., Sherman, N. E., Langer, R. S., & Karp, J. M. (2018). Towards a defined ECM and small molecule based monolayer culture system for the expansion of mouse and human intestinal stem cells. *Biomaterials*, *154*, 60–73. https://doi.org/10.1016/j.biomaterials.2017.10.038

bioRxiv preprint doi: https://doi.org/10.1101/2025.04.17.649452; this version posted April 23, 2025. The copyright holder for this preprint (which was not certified by peer review) is the author/funder, who has granted bioRxiv a license to display the preprint in perpetuity. It is made available under a CC-BY-NC-ND 4.0 International license.

724 Tuftee, C., Alsberg, E., Ozbolat, I. T., & Rizwan, M. (2024). Emerging granular hydrogel bioinks to
725 improve biological function in bioprinted constructs. *Trends in Biotechnology*, *42*(3), 339–
726 352. https://doi.org/10.1016/j.tibtech.2023.09.007
727 Ushakov, R., Ratushnyy, A., Buravkova, L., Tolkunova, E., & Burova, E. (2024). The Decellularized
728 Cell-Derived Extracellular Matrix Enhances the Paracrine Function of Human Mesenchymal
729 Stromal/Stem Cells. *International Journal of Molecular Sciences*, *25*(4), Article 4.
730 https://doi.org/10.3390/ijms25042419
731 Wiese, D. M., & Braid, L. R. (2020). Transcriptome profiles acquired during cell expansion and
732 licensing validate mesenchymal stromal cell lineage genes. *Stem Cell Research and Therapy*,
733 *11*(1), 1–7. https://doi.org/10.1186/S13287-020-01873-7/FIGURES/3
734 Wiese, D. M., Wood, C. A., Ford, B. N., & Braid, L. R. (2022). Cytokine Activation Reveals Tissue-
735 Imprinted Gene Profiles of Mesenchymal Stromal Cells. *Frontiers in Immunology*, *13*.
736 https://www.frontiersin.org/articles/10.3389/fimmu.2022.917790
737 Wilks, B. T., Evans, E. B., Nakhla, M. N., & Morgan, J. R. (2018). Directing fibroblast self-assembly
738 to fabricate highly-aligned, collagen-rich matrices. *Acta Biomaterialia*, *81*, 70–79.
739 https://doi.org/10.1016/j.actbio.2018.09.030
740 Yang, M. C., Chin, I. L., Fang, H., Drack, A., Nour, S., Choi, Y. S., O'Connor, A. J., Greening, D.
741 W., Kalionis, B., & Heath, D. E. (2024). Tailored environments for directed mesenchymal
742 stromal cell proliferation and differentiation using decellularized extracellular matrices in
743 conjunction with substrate modulus. *Acta Biomaterialia*, *187*, 110–122.
744 https://doi.org/10.1016/j.actbio.2024.08.022
745 Yin, S., Wu, H., Huang, Y., Lu, C., Cui, J., Li, Y., Xue, B., Wu, J., Jiang, C., Gu, X., Wang, W., &
746 Cao, Y. (2024). Structurally and mechanically tuned macroporous hydrogels for scalable

bioRxiv preprint doi: https://doi.org/10.1101/2025.04.17.649452; this version posted April 23, 2025. The copyright holder for this preprint (which was not certified by peer review) is the author/funder, who has granted bioRxiv a license to display the preprint in perpetuity. It is made available under a CC-BY-NC-ND 4.0 International license.

mesenchymal stem cell–extracellular matrix spheroid production. *Proceedings of the National Academy of Sciences*, *121*(28), e2404210121. https://doi.org/10.1073/pnas.2404210121

Zhang, X., Battiston, K. G., Labow, R. S., Simmons, C. A., & Santerre, J. P. (2017). Generating favorable growth factor and protease release profiles to enable extracellular matrix accumulation within an *in vitro* tissue engineering environment. *Acta Biomaterialia*, *54*, 81–94. https://doi.org/10.1016/j.actbio.2017.02.041

Zhang, Y., Feng, Y., Shao, Q., Jiang, Z., & Yang, G. (2023). Rapid formation of 3D: Decellularized extracellular matrix spheroids for enhancing bone formation. *Journal of Biomedical Materials Research. Part A*, *111*(3), 378–388. https://doi.org/10.1002/jbm.a.37471

Zhao, W., Zhu, J., Hang, J., & Zeng, W. (2022). Biomaterials to promote vascularization in tissue engineering organs and ischemic fibrotic diseases. *MedComm – Biomaterials and Applications*, *1*(1), e16. https://doi.org/10.1002/mba2.16

bioRxiv preprint doi: https://doi.org/10.1101/2025.04.17.649452; this version posted April 23, 2025. The copyright holder for this preprint (which was not certified by peer review) is the author/funder, who has granted bioRxiv a license to display the preprint in perpetuity. It is made available under a CC-BY-NC-ND 4.0 International license.

772